

Hadronic resonance production with ALICE at the LHC

S. Kiselev^{a1} for the ALICE Collaboration

^a NRC “Kurchatov Institute”, Moscow, Russia

Recent results on short-lived hadronic resonances obtained with the ALICE detector at LHC energies are presented. These results include masses, widths, transverse momentum spectra, yields, and ratios of resonance yields to longer-lived ground-state particles, and elliptic flows. The results are compared with model predictions and measurements at lower energies.

PACS: 25.75.Gz; 13.25.-k; 13.30.Eg

The study of resonance production is important in proton-proton, proton-nucleus, and heavy-ion collisions. Since the lifetimes of short-lived resonances are comparable with the lifetime of the late hadronic phase produced in heavy-ion collisions, resonance yields are affected by the regeneration and rescattering of their decay daughters in the hadronic phase. These competing effects are investigated by measuring the yield ratios of resonances to that of the ground-state longer-lived hadron as a function of charged-particle multiplicity. From these measurements, it is possible to obtain information on the time interval between the chemical and the kinetic freeze-out. Measurements in pp and p-Pb collisions constitute a reference for nuclear collisions and provide information for tuning event generators inspired by Quantum Chromodynamics. Moreover, some heavy-ion effects (elliptic flow [1]- [2], strangeness enhancement [3]) were also unexpectedly observed in small collision systems.

Results on short-lived mesonic $\rho(770)^0$, $K^*(892)^0$, $K^*(892)^\pm$, $f_0(980)$, $\phi(1020)$, $f_1(1275)$ as well as baryonic $\Sigma(1385)^\pm$, $\Lambda(1520)$, $\Xi(1530)^0$ and $\Omega(2012)^-$ resonances (hereafter denoted as ρ^0 , K^{*0} , $K^{*\pm}$, f_0 , ϕ , f_1 , $\Sigma^{*\pm}$, Λ^* , Ξ^{*0} , Ω^*) have been obtained using data reconstructed with the ALICE detector. The resonances are reconstructed in their hadronic decay channels and have very different lifetimes as shown in Table 1.

This contribution reports recent results obtained for f_1 [29], Ω^* [32], $K^{*\pm}$ [21] and f_0 [24] in pp collisions at 13 TeV, for K^{*0} and ϕ in Pb-Pb collisions at 5.36 TeV, and for $f_0(1710)$ in pp collisions at 13.6 TeV.

The first measurement of the f_1 meson has been made in pp collisions at $\sqrt{s} = 13$ TeV. The mass of f_1 is in reasonable agreement with the world-average value, Fig. 1 (top, left). Figure 1 (top, right) shows the p_T spectrum with a fit by a Lévy-Tsallis function, to extrapolate the yield down to zero p_T and extract the p_T -integrated yield dN/dy and the average transverse momentum $\langle p_T \rangle$. Since there are only two p_T bins above 6 GeV/c with large bin width, the Lévy-Tsallis fit in the default case is performed in the

¹E-mail: Sergey.Kiselev@cern.ch

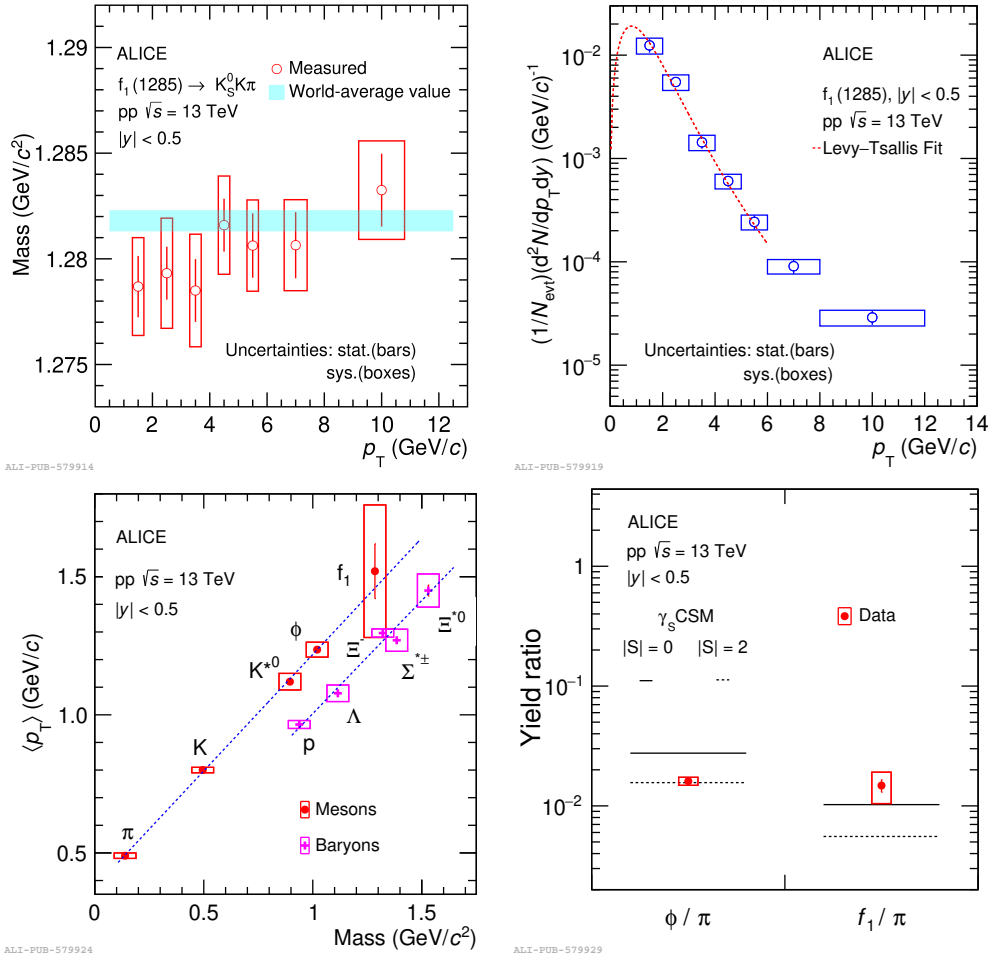


Fig. 1. Mass (top, left) and p_T -differential yield (top, right) of the f_1 . The p_T spectrum is fitted by a Levy-Tsallis [35] function. (bottom, left) The average transverse momentum of f_1 with that of all other light flavor hadrons [14], [27]. (bottom, right) The particle yield ratios ϕ/π [14] and f_1/π with model predictions from γ_S -CSM [36].

Table 1. Lifetime values [4], reconstructed decay mode, reactions and the corresponding references where ALICE results for the hadronic resonances are reported.

Resonance	$c\tau(fm)$	Decay	System @ energy(TeV)	ALICE papers
ρ^0	1.3	$\pi\pi$	pp/p-Pb @ 2.76	[5]
K^{*0}	4.3	$K\pi$	pp/p-Pb/Pb-Pb/Xe-Xe @ all energies	[6]- [18]
$K^{*\pm}$	4.3	$K_S^0\pi$	pp @ 5.02/8/13 Pb-Pb @ 5.02	[19]- [21]
f_0	~ 5	$\pi\pi$	pp/p-Pb @ 5.02	[22]- [24]
$\Sigma^{*\pm}$	5-5.5	$\Lambda\pi$	pp @ 7/13 p-Pb/Pb-Pb @ 5.02	[25]- [28]
f_1	8.7	$K_S^0K\pi$	pp @ 13	[29]
Λ^*	12.6	pK	pp @ 7 p-Pb @ 5.02 Pb-Pb @ 5.02	[30]- [31]
Ξ^{*0}	21.7	$\Xi\pi$	pp @ 7/13 p-Pb @ 5.02	[25]- [27]
Ω^*	32.3	ΞK_S^0	pp @ 13	[32]
ϕ	46.2	KK	pp/p-Pb/Pb-Pb/Xe-Xe @ all energies	[6]- [17], [33]- [34]

$0 < p_T < 6$ GeV/ c range. The extrapolation to the low p_T (< 1 GeV/ c) region encompasses approximately 41% of the total f_1 yield. The high p_T extrapolation is found to be negligible. Figure 1 (bottom, left) compares the average transverse momentum of f_1 with that of all other light flavor hadrons. For particles with similar masses, mesons exhibit a higher average transverse momentum than baryons. Notably, f_1 aligns with the linear trend of other mesons, although with large conservative systematic uncertainties. This observation suggests that f_1 may have an ordinary meson structure. Figure 1 (bottom, right) shows the particle yield ratios ϕ/π and f_1/π with model predictions from γ_S -CSM for $|S|=0$ (zero strangeness content) and $|S|=2$ (hidden strangeness content). As expected, for ϕ/π the ratio with $|S|=2$ is in good agreement with the data. For f_1/π , the ratio with $|S|=0$ agrees with the data within 1σ , and with $|S|=2$ deviates by $\sim 2\sigma$, suggesting that f_1 is a conventional non-strange meson.

A signal consistent with the Ω^* baryon has been observed with a significance of 15σ in high-multiplicity-triggered (HM) pp collisions at $\sqrt{s} = 13$ TeV. Figure 2 shows the mass and width of Ω^* . These values are consistent with the previous measurements by Belle. The first measurement of transverse-momentum spectrum has been made. The Ω^* transverse-momentum spectrum, not corrected for the unmeasured $\Omega^* \rightarrow \Xi K_S^0$ branching ratio, is shown in Fig. 3. The spectrum is fitted with the parameterized spectrum function, with only the overall scale factor allowed to vary.

Figure 4 (left) shows the multiplicity dependence of the $K^{*\pm}/K$ ratio in pp collisions at $\sqrt{s} = 13$ TeV, compared to the K^{*0}/K ratio. The decreasing trend already outlined by the K^{*0} analysis is confirmed by the $K^{*\pm}$ results. The $K^{*\pm}/K$ ratio in the highest multiplicity class is lower than the low multiplicity value at $\sim 7\sigma$ level taking into account the multiplicity uncorrelated uncertainties ($\sim 2\sigma$ level for the K^{*0}/K ratio). This result represents the

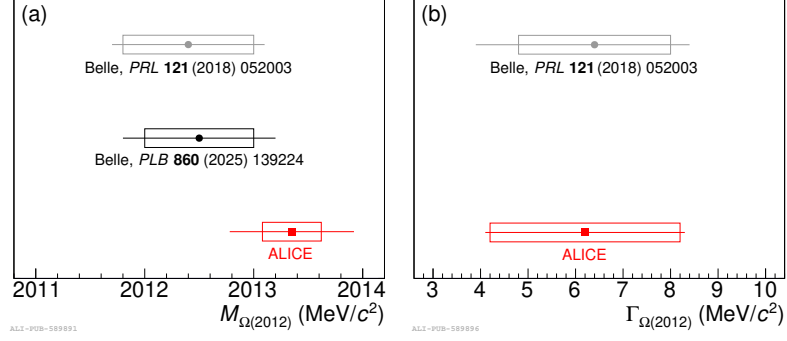


Fig. 2. Mass (a) and width (b) of the Ω^* . Results of Belle [37], [38] are also shown.

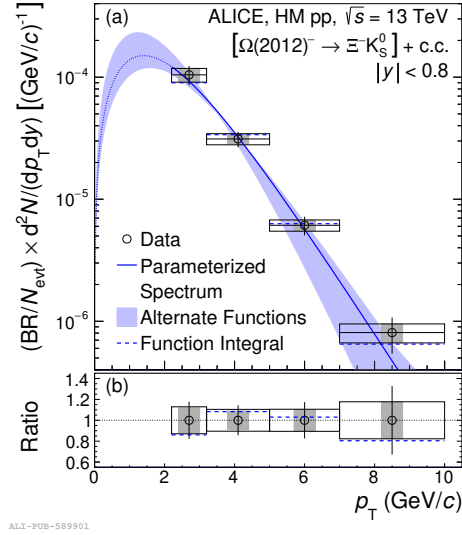


Fig. 3. (a) The transverse-momentum spectrum of the Ω^* in HM pp collisions at $\sqrt{s} = 13$ TeV (not corrected for the unmeasured branching ratio BR for the studied decay channel). The shaded band surrounding the curve indicates the region spanned by the envelope of alternate functions used to describe the spectrum, which affect the extrapolation of the yield to low p_T . (b) The ratio of the parameterized yield to the measured yield.

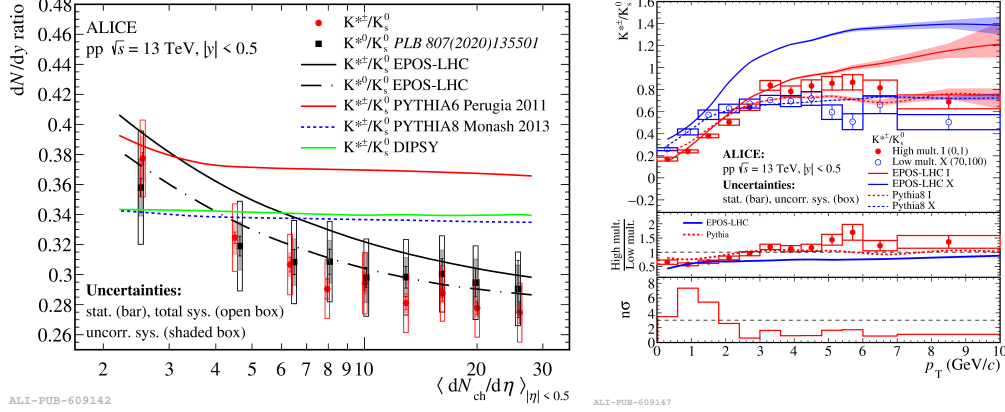


Fig. 4. (color online) Left: Ratios K^{\pm}/K and K^0/K [12] as a function of the charged-particle multiplicity density in pp collisions at $\sqrt{s} = 13$ TeV. Model predictions from PYTHIA6 [39], PYTHIA8 [40], EPOS-LHC [41] and DIPSY [42] are also shown. Right: Ratios K^{\pm}/K as a function of p_T for low (X) and high (I) multiplicity classes.

first evidence of a clear K^*/K suppression measured in small collision systems. EPOS-LHC provides good agreement with the measured data, well reproducing the decreasing trend, while PYTHIA6, PYTHIA8 and DIPSY tend to overestimate the ratios at high multiplicities and exhibit a fairly flat trend. It is worth noting that none of these event generators consider the evolution of a hadronic phase or the eventual hadronic interactions of generated particles. The ratio of the high multiplicity K^{\pm}/K differential p_T distribution to the low multiplicity one helps to quantify the observed decrease in the particle ratios, Fig. 4 (right). For $p_T \leq 2$ GeV/c, the double K^{\pm}/K ratio deviates from unity by more than 3σ , suggesting a low p_T dominant process.

Figure 5 demonstrates the double ratios of f_0 to π (left) and K^0 (right) as a function of multiplicity in pp collisions at $\sqrt{s} = 13$ TeV. The f_0/π suppression could be explained by the dominance of the rescattering effect. The double ratio f_0/K^0 also decreases with increasing multiplicity. Even if rescattering affects both f_0 and K^0 , these resonances, which have similar lifetimes, differ by their decay daughters: (π, π) for f_0 and (K, π) for K^0 . The rescattering effect for f_0 can be stronger than for K^0 if the cross section $\sigma(\pi\pi) > \sigma(K\pi)$. The γ_S -CSM (where rescattering is not implemented) predictions with $|S|=0$ scenario are closer to the data values. However, the model does not reproduce the ratios at low multiplicity, in contrast to other hadrons [36].

Figure 6 shows the ϕ and K^0 meson elliptic flow as a function of p_T in Pb-Pb collisions at $\sqrt{s_{NN}} = 5.36$ TeV, along with the ALICE measurements for other hadrons in Pb-Pb collisions at $\sqrt{s_{NN}} = 5.02$ TeV for centrality class 30–40%. Both K^0 and ϕ follow mass ordering at low $p_T \leq 3$ GeV/c and baryon-meson grouping at intermediate p_T . These observations confirm

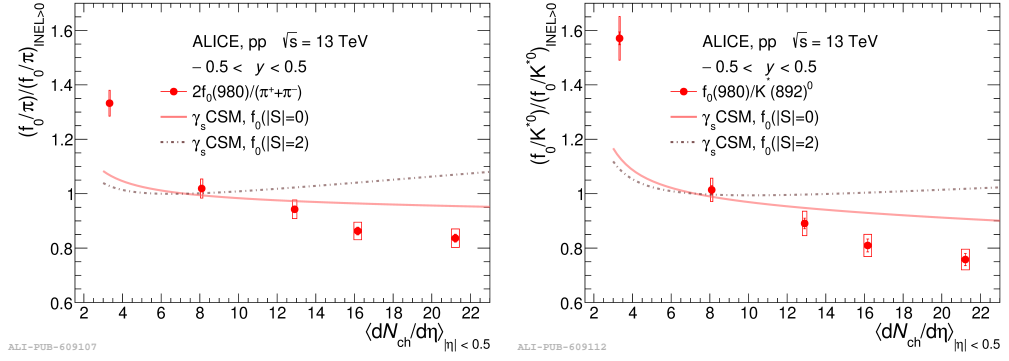


Fig. 5. Double ratios of f_0 to π (left) and K^{*0} (right) as a function of multiplicity in pp collisions at $\sqrt{s_{NN}} = 13$ TeV. Model predictions from γ_s -CSM [36] are also shown.

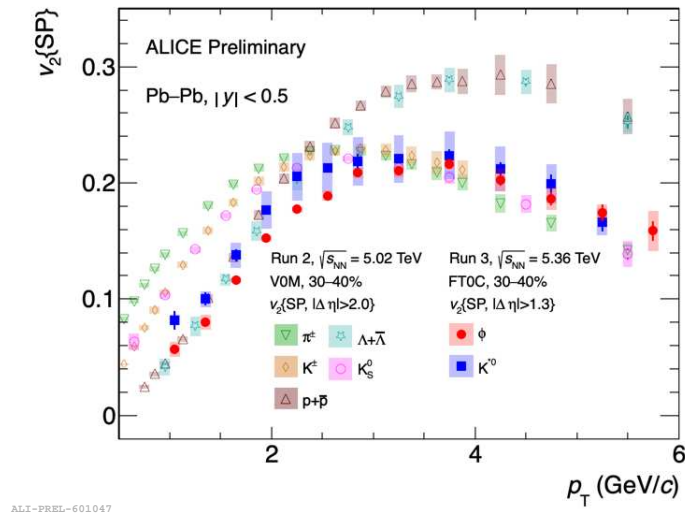


Fig. 6. The elliptic flow for ϕ and K^{*0} in Pb-Pb collisions at $\sqrt{s_{NN}} = 5.36$ TeV from Run 3. Measurements for other hadrons from Run 2 [33] are also shown.

that both the K^{*0} and ϕ mesons participate in the collective expansion of the medium and undergo hadronization via quark coalescence in quark-gluon plasma.

Figure 7 (left) presents the $K_S^0 K_S^0$ invariant mass distribution in pp collisions at $\sqrt{s} = 13.6$ TeV. The $f_0(1710)$ meson is observed. It can be the light-

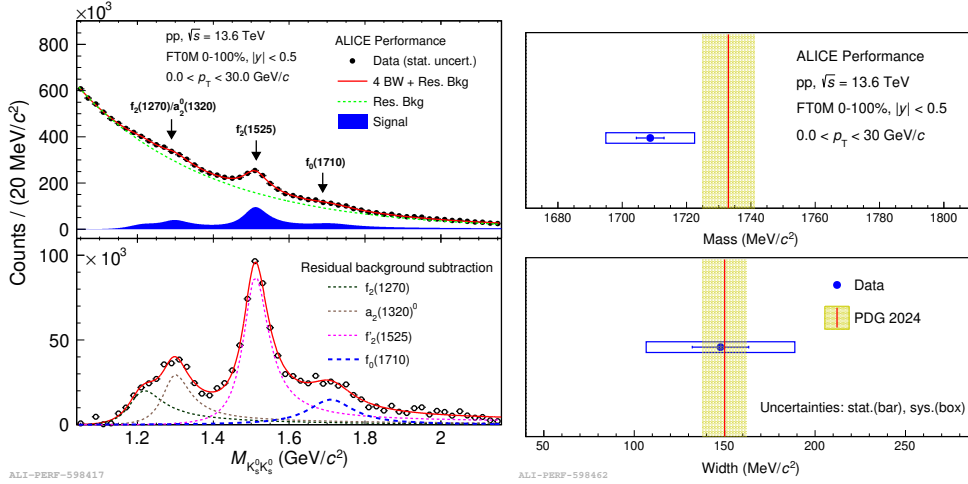


Fig. 7. Left: Background subtracted $K_S^0 K_S^0$ invariant mass distribution in pp collisions at $\sqrt{s} = 13.6$ TeV. Right: Mass and width of $f_0(1710)$.

est scalar glueball candidate predicted by QCD [43]. The mass of $f_0(1710)$ is within 1.5σ of the PDG value, the width aligns with the PDG value (Fig. 7, right).

In summary, recent results on short-lived hadronic resonances f_1 , Ω^* , $K^{*\pm}$ and f_0 in pp collisions at $\sqrt{s} = 13$ TeV, K^{*0} , ϕ in Pb-Pb at $\sqrt{s_{NN}} = 5.36$ TeV, and $f_0(1710)$ in pp at 13.6 TeV have been presented. The average transverse momentum of f_1 aligns with the linear trend with mass observed for other mesons. This observation suggests that f_1 may have an ordinary meson structure. The γ_S -CSM model prediction with $|S|=0$ (zero strangeness content) for the f_1/π ratio agrees with the data within 1σ and with $|S|=2$ (hidden strangeness content) deviates by $\sim 2\sigma$ suggesting that f_1 is a conventional meson. The mass and width of Ω^* are consistent with the previous measurements by Belle. Firstly the transverse-momentum spectrum of the Ω^* has been measured. The $K^{*\pm}/K$ ratio in the highest multiplicity class is lower than the low multiplicity value at $\sim 7\sigma$ level representing the first evidence of a K^*/K suppression measured in pp collisions. The EPOS-LHC model without any hadronic afterburner is able to reproduce the measured suppression. Both the f_0/π and f_0/K^{*0} ratios decrease with increasing multiplicity. The f_0/π suppression could be explained by the dominance of the rescattering effect. The rescattering effect for f_0 can be stronger than for K^{*0} if cross section $\sigma(\pi\pi) > \sigma(K\pi)$. For both resonances γ_S -CSM (no rescattering effect) predictions with $|S|=0$ scenario are closer to the data values. The elliptic flow for ϕ and K^{*0} follow mass ordering at low $p_T \leq 3$ GeV/c and baryon-meson

grouping at intermediate p_T . These observations confirm that both the K^{*0} and ϕ mesons participate in the collective expansion of the medium and undergo hadronization via quark coalescence in quark–gluon plasma. The mass of $f_0(1710)$ is within 1.5σ of the PDG value, the width aligns with the PDG value.

FUNDING

The work was carried out within the state assignment of NRC “Kurchatov Institute”.

CONFLICT OF INTEREST

The author of this work declares that he has no conflicts of interest.

REFERENCES

1. Acharya S *et al.* (ALICE Collaboration) 2019 *Phys. Rev. Lett.* **123** 142301.
2. ALICE Collaboration, arXiv:2411.09323 [nucl-ex].
3. Adam J *et al.* (ALICE Collaboration) 2013 *Nature Phys.* **13** 535.
4. Navas S *et al.* (Particle Data Group) 2024 *Phys. Rev. D* **110** 030001.
5. Acharya S *et al.* (ALICE Collaboration) 2019 *Phys. Rev. C* **99** 064901.
6. Abelev B *et al.* (ALICE Collaboration) 2012 *Eur. Phys. J. C* **72** 2183.
7. Abelev B *et al.* (ALICE Collaboration) 2015 *Phys. Rev. C* **91** 024609.
8. Adam J *et al.* (ALICE Collaboration) 2016 *Eur. Phys. J. C* **76** 245.
9. Adam J *et al.* (ALICE Collaboration) 2017 *Phys. Rev. C* **95** 064606.
10. Acharya S *et al.* (ALICE Collaboration) 2019 *Phys. Rev. C* **99** 024906.
11. Acharya S *et al.* (ALICE Collaboration) 2020 *Phys. Lett. B* **802** 135225.
12. Acharya S *et al.* (ALICE Collaboration) 2020 *Phys. Lett. B* **807** 135501.
13. Acharya S *et al.* (ALICE Collaboration) 2020 *Phys. Rev. C* **102** 024912.
14. Abelev B *et al.* (ALICE Collaboration) 2021 *Eur. Phys. J. C* **81** 256.
15. Acharya S *et al.* (ALICE Collaboration) 2022 *Phys. Rev. C* **106** 034907.
16. Acharya S *et al.* (ALICE Collaboration) 2023 *Phys. Rev. C* **107** 055201.
17. Acharya S *et al.* (ALICE Collaboration) 2023 *Eur. Phys. J. C* **83** 540.

18. Acharya S *et al.* (ALICE Collaboration) 2024 *Phys. Rev. C* **109** 014911.
19. Acharya S *et al.* (ALICE Collaboration) 2022 *Phys. Lett. B* **828** 137013.
20. Acharya S *et al.* (ALICE Collaboration) 2024 *Phys. Rev. C* **109** 044902.
21. ALICE Collaboration, arXiv:2507.19332 [nucl-ex].
22. Acharya S *et al.* (ALICE Collaboration) 2023 *Phys. Lett. B* **846** 137644.
23. Acharya S *et al.* (ALICE Collaboration) 2024 *Phys. Lett. B* **853** 138665.
24. ALICE Collaboration, arXiv:2507.19347 [nucl-ex].
25. Abelev B *et al.* (ALICE Collaboration) 2015 *Eur. Phys. J. C* **75** 1.
26. Adamova D *et al.* (ALICE Collaboration) 2017 *Eur. Phys. J. C* **77** 389.
27. Acharya S *et al.* (ALICE Collaboration) 2024 *J. High Energy Phys.* **5** 317.
28. Acharya S *et al.* (ALICE Collaboration) 2023 *Eur. Phys. J. C* **83** 351.
29. Acharya S *et al.* (ALICE Collaboration) 2025 *Phys. Lett. B* **866** 139562.
30. Acharya S *et al.* (ALICE Collaboration) 2019 *Phys. Rev. C* **99** 024905.
31. Acharya S *et al.* (ALICE Collaboration) 2020 *Eur. Phys. J. C* **80** 160.
32. ALICE Collaboration, arXiv:2502.18063 [hep-ex].
33. Acharya S *et al.* (ALICE Collaboration) 2018 *J. High Energy Phys.* **09** 006.
34. Acharya S *et al.* (ALICE Collaboration) 2021 *Eur. Phys. J. C* **81** 584.
35. C. Tsallis, *J. Stat. Phys.* **52** (1988) 479.
36. Vovchenko V, Donigus B, and Stoecker H 2019 *Phys. Rev. C* **100** 054906.
37. Yelton J *et al.* (Belle Collaboration) 2018 *Phys. Rev. Lett.* **121** 052003.
38. Jia S *et al.* (Belle Collaboration) 2025 *Phys. Lett. B* **860** 139224.
39. Skands P Z 2010 *Phys. Rev. D* **82** 074018.
40. Skands P Z *et al.* 2014 *Eur. Phys. J. C* **74** 3024.
41. Pierog T *et al.* 2016 *Phys. Rev. C* **92** 034906.
42. Flensburg C *et al.* 2011 *J. High Energy Phys.* **8** 103.
43. Chen Y *et al.* 2006 *Phys. Rev. D* **73** 014516.